Structural Behaviour of Precast Beam-Column Sub-Assemblages with Cast-In-Situ Engineered Cementitious Composites under Column Removal Scenarios

Kang, Shao-Bo; Tan, Kang Hai; Yang, En-Hua; Ng, Kian Wee

2015

Kang, S.-B., Tan, K. H., Yang, E.-H., & Ng, K. W. (2015). Structural behaviour of precast beam-column sub-assemblages with cast-In-situ engineered cementitious composites under column removal scenarios. 5thInternational Conference on Design and Analysis of Protective Structures (DAPS2015), 1-9.

https://hdl.handle.net/10356/80678

Structural Behaviour of Precast Beam-Column Sub-Assemblages with Cast-In-Situ Engineered Cementitious Composites under Column Removal Scenarios

Shao-Bo Kang[1], Kang Hai Tan[1], En-Hua Yang[1], Kian Wee Ng[2]

[1] *School of Civil & Environmental Engineering, Nanyang Technological University, 50 Nanyang Avenue, 639798 Singapore* (skang2@e.ntu.edu.sg, CKHTAN@ntu.edu.sg, EHYANG@ntu.edu.sg)
[2] *Civil and Structural Engineering Department, JTC Corporation, 8 Jurong Town Hall Road, 609434 Singapore* (NG_Kian_Wee@jtc.gov.sg)

Abstract

This paper presents an experimental study on the structural behaviour of precast beam-column sub-assemblages under column removal scenarios, in which conventional concrete and engineered cementitious composites (ECC) were used in the cast-in-situ concrete topping and the beam-column joint. The specimens were restrained by horizontal and vertical load cells and tested under quasi-static loading condition. Experimental results indicate that at the initial stage ECC and steel reinforcement sustained tensile stresses compatibly and multiple cracking was observed in the ECC topping. When the tensile strain capacity of ECC was exhausted, major cracks were formed in the plastic hinge region, whereas at other sections ECC remained intact to transfer tensile stresses across cracks. Compared to conventional concrete, ECC resulted in more severe localisation of rotations in a limited region due to its tension-stiffening behaviour. Conclusions are drawn that application of ECC to structural topping and beam-column joints did not significantly enhance structural resistance of sub-assemblages under column removal scenarios. However, the calculated pseudo-static resistance of ECC sub-assemblage is greater than that of concrete specimen due to better energy-absorption capacity of ECC.

Keyword: Column removal scenarios, Beam-column sub-assemblages, Engineered cementitious composites, Compressive arch action, Catenary action

1. Introduction

To develop alternate load paths under column removal scenarios, the bridging beam has to experience significant deformations, which poses high requirements on the ductility and robustness of beam-column joints. Reinforced concrete beam-column joints are able to redistribute vertical load through compressive arch action and catenary action if one supporting column is removed without any damage to other structural members and joints [1]. In precast concrete structures, welded joints are vulnerable to progressive collapse due to the reduced ductility of reinforcement in the heat-affected zone [2]. Through proper reinforcement detailing, such as lap-splice or hooked anchorage in the beam-column joint, equivalent behaviour to monolithic joints can be achieved in precast concrete joints under earthquake loads [3]. However, the behaviour of precast concrete joints under column removal scenarios remains a concern and has not been investigated yet. On top of special reinforcement detailing in the joint, innovation of ductile concrete materials in recent years, such as engineered cementitious composites (ECC), provides an alternative way to potentially enhance structural performance under progressive collapse scenarios.

As a fibre-reinforced concrete, engineered cementitious composites (ECC) is characterised by strain-hardening behaviour and ultra-high strain capacity in tension [4]. With a fibre content of 2%, the strain capacity of ECC can be up to 5%, several hundred times higher than that of conventional concrete. As for reinforced ECC members in uniaxial tension, compatible deformations between ECC and steel reinforcement can be obtained at small deformation [5]. However, at large deformation stage,

ductility of embedded reinforcement is substantially reduced due to tension-stiffening behaviour of ECC [6]. Therefore, potential application of ECC to precast beam-column sub-assemblages under column removal scenarios has to be studied through experimental tests.

This paper presents an experimental investigation on the behaviour of precast beam-column sub-assemblages with 90^o bend of bottom reinforcement in the beam-column joint under column removal scenarios. Besides conventional concrete, ECC was used in structural topping and beam-column joints. An attempt was made to quantify the potential enhancement of ECC to structural resistance and deformation capacity of sub-assemblages.

2. Experimental Programme

In the experimental programme, a precast concrete structure was designed against gravity load in accordance with Eurocode 2 [7]. One middle supporting column was assumed to be forcibly removed with any damage to remaining structural members and beam-column joints, as prescribed by UFC 4-023-03 [8]. A beam-column sub-assemblage immediately over the removed column, comprising a middle beam-column joint and a two-span bridging beam, was extracted from the precast concrete structure and tested under quasi-static loading condition. To facilitate installation of horizontal and vertical restraints to the bridging beam, two enlarged column stubs were erected at two ends of the beam. Fig. 1 shows the geometry and reinforcement detail of sub-assemblage CMJ-B-1.19/0.59.

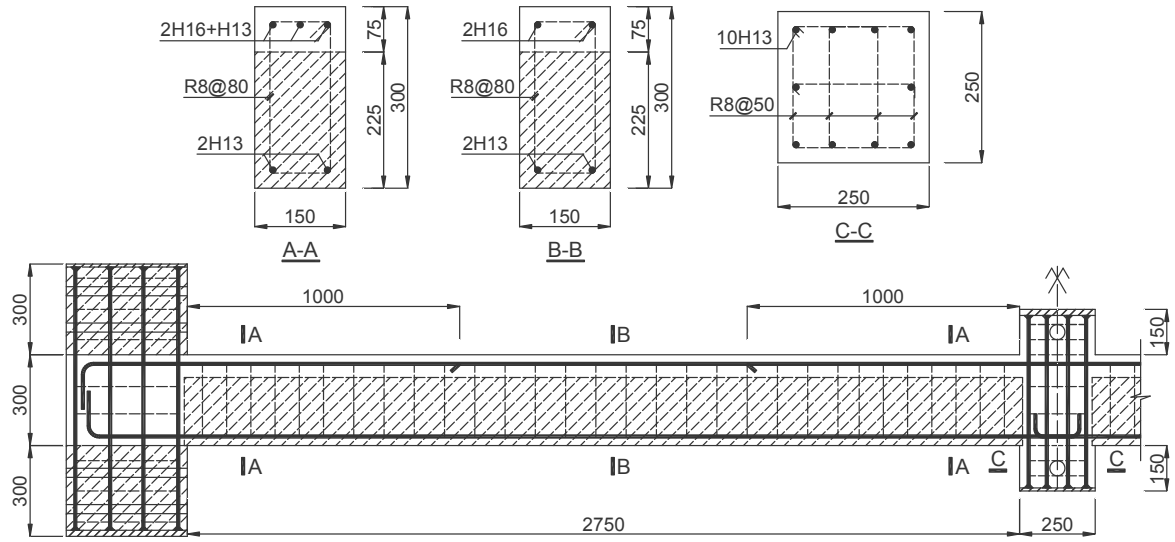

Fig. 1: Geometry and reinforcement detailing of beam-column sub-assemblage CMJ-B-1.19/0.59

Table 1: Reinforcement detail of beam-column sub-assemblages

Sub-assemblages	Section A-A		Section B-B		Stirrups	Material	
	Top	Bottom	Top	Bottom		Precast beam	Joint
CMJ-B-1.19/0.59	2H16+H13 (1.19%)	2H13 (0.59%)	2H16 (0.90%)	2H13 (0.59%)	R8@80	Concrete	Concrete
EMJ-B-1.19/0.59							ECC

Precast concrete structures feature weak beam-column joints due to discontinuity of longitudinal reinforcement in the joints. Thus, reinforcement detailing in the beam-column joint plays a crucial role in the behaviour of sub-assemblages under column removal scenarios. In this study, 90^o bend of bottom reinforcement was used in the beam-column joint, as shown in Fig. 1. Beam units were prefabricated, as shown by hatched zones in Fig. 1. Thereafter, the precast beam units were assembled with continuous top reinforcement through the middle joint, as specified by Van Acker [9], to form an integral sub-assemblage. Finally, in-situ concrete was cast in the structural topping and the beam-column joint. To study the effect of ECC on the behaviour of sub-assemblages, ECC was used in the structural topping and the beam-column joints of EMJ-B-1.19/0.59 in place of conventional concrete,

as included in Table 1. To ensure horizontal shear transfer between precast beam units and cast-in-situ concrete topping, adequate stirrups with 8 mm diameter at 80 mm spacing were provided in the beam.

Fig. 2 shows the test set-up for beam-column sub-assemblages. Restraints to the bridging beam from adjacent structural members were decomposed into two horizontal restraints and one vertical support at each end column stub. Reaction forces were measured through load cells in the restraints. Additionally, two pairs of short steel columns were used by the side of the beam to prevent out-of-plane deflection of the beam. In the middle joint, a rotational restraint was designed to avert rotation of the joint after fracture of bottom reinforcement occurred at one side of the joint. Displacement-controlled vertical load was applied to the middle joint at a rate of 6 mm/min. During the test, vertical deflections of beam-column sub-assemblages were captured through linear variable differential transducers (LVDTs) under the beam, as shown in Fig. 3. Rotations of plastic hinges at the middle joint and the end column stub were also measured through two rows of LVDTs at the beam ends to quantify the deformation capacity of sub-assemblages.

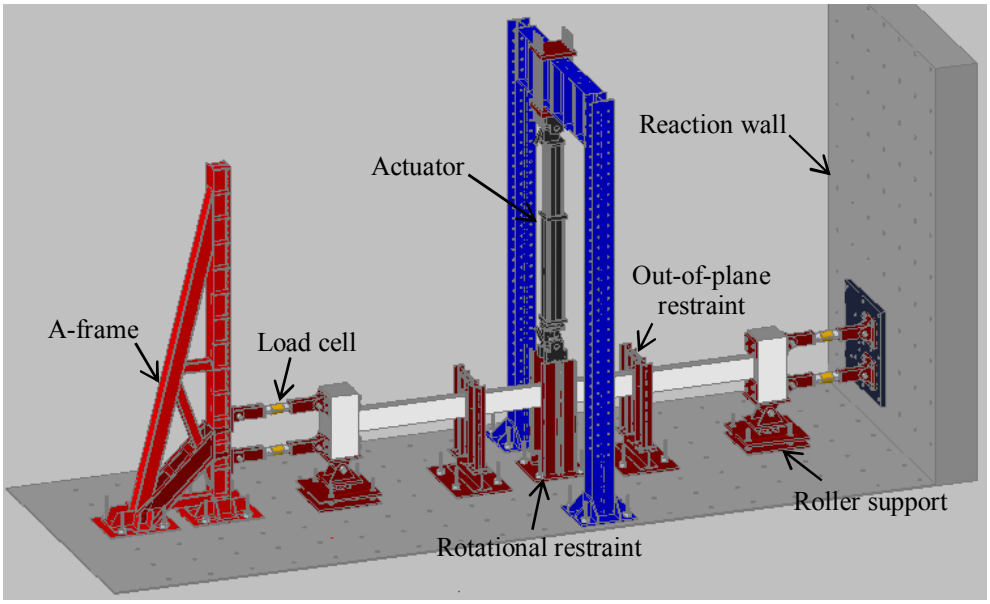

Fig. 2: Test set-up for beam-column sub-assemblage

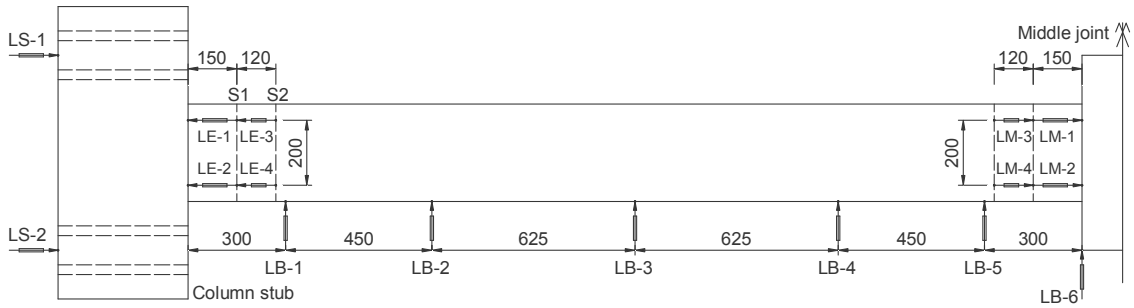

Fig. 3: Layout of LVDTs on sub-assemblages

3. Material Properties

High-strength deformed reinforcement H13 and H16 was used for longitudinal reinforcement in the beam, and round bars R8 were used for stirrups. Material tests were conducted on steel reinforcing bars with a gauge length of 300 mm. Table 2 shows the material properties of reinforcement. Besides, concrete cylinders with dimensions of 150 diameter and 300 mm long were tested and compressive strength of concrete was obtained (see Table 2). As for ECC, the compressive strength obtained from 50 mm cube was 62.7 MPa. Four-point bending tests were also conducted for ECC plates with dimensions of 300 mm long by 70 mm wide by 12 mm thick. The clear span between two supports

was 240 mm. Fig. 4 shows the load-deflection curve of one ECC plate. After cracking, applied load increased with deflection, indicating significant hardening behaviour under bending. Correspondingly, the effective tensile strength was determined as 3.1 MPa and the tensile strain capacity was calculated as 2.6% in accordance with inverse analysis [10, 11].

Table 2: Material properties of reinforcing and concrete

Steel reinforcement		Yield Strength (MPa)	Modulus of elasticity (GPa)	Ultimate strength (MPa)	Fracture strain (%)
Longitudinal reinforcement	H13	549	206.6	698	16.3
	H16	573	211.3	674	12.9
Stirrup	R8	270	202.5	371	27.5
Concrete		Compressive strength (MPa)		Secant modulus (GPa)	
Precast beam unit		40.5		29.2	
Cast-in-situ concrete topping (CMJ-B-1.19/0.59 only)		36.1		31.4	

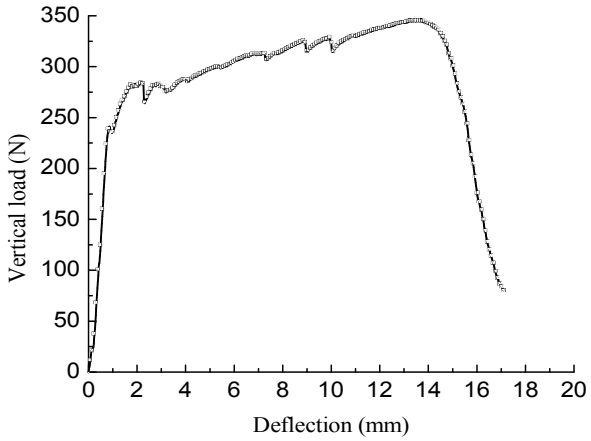

Fig. 4: Load-deflection curve of ECC plate under four-point bending

4. Quasi-Static Resistance of Beam-Column Sub-Assemblages

Figs. 5(a and b) show the variations of vertical loads and horizontal reaction forces with middle joint displacement. At the initial stage, vertical load on the middle joint was resisted by compressive arch action which features axial compression force in the bridging beam, as shown in Fig. 5(b). The compressive arch action capacity of sub-assemblage CMJ-B-1.19/0.59 was 90.4 kN. Beyond the load capacity at the compressive arch action stage, vertical load decreased with increasing middle joint displacement due to crushing of concrete in the compression zone of the beam. At around 230 mm displacement, fracture of bottom reinforcement occurred at the face of the middle joint, leading to a sudden drop of the vertical load (see Fig. 5(a)). Thereafter, vertical load started increasing due to the presence of rotational restraint in the middle joint. When the displacement surpassed one beam depth 300 mm, catenary action kicked in and the beam sustained vertical load through its axial tension force, as shown in Fig. 5(b). Final failure of sub-assemblages was caused by fracture of top longitudinal reinforcement near the end column stub. The catenary action capacity of CMJ-B-1.19/0.59 was attained as 108.2 kN, around 20% higher than the compressive arch action capacity. Sub-assemblage EMJ-B-1.19/0.59 developed nearly the same capacities at the compressive arch action and catenary action stage, as shown in Fig. 5(a). The compressive arch action and catenary action capacities were 91.1 kN and 110.3 kN, respectively. Compared to CMJ-B-1.19/0.59, ECC in structural topping and beam-column joints did not significantly enhance structural resistance of EMJ-B-1.19/0.59 under column removal scenarios.

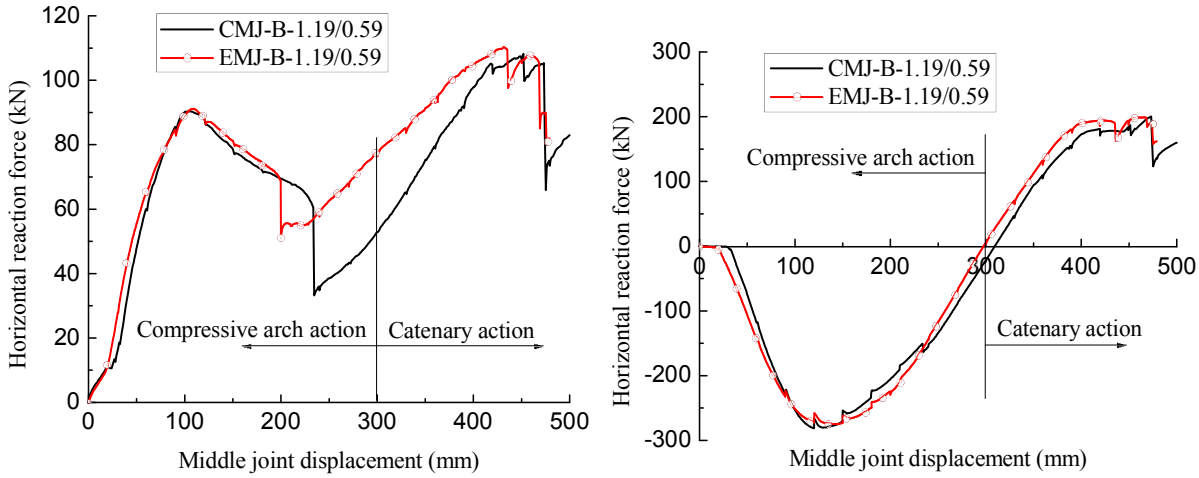

Fig. 5: Variations of vertical loads and horizontal reaction forces with middle joint displacement

At compressive arch action stage, axial compression force developed in the bridging beam, as shown in Fig. 5(b). The maximum compression forces in sub-assemblages CMJ-B-1.19/0.59 and EMJ-B-1.19/0.59 were 281.1 kN and 274.7 kN, respectively. Development of compression force in the beam substantially increased the resistance of sub-assemblages. For instance, based on plastic hinge mechanism, the capacity of sub-assemblage CMJ-B-1.19/0.59 can be calculated as 74.3 kN under flexural action. Axial compression force in the beam increased the flexural resistance of CMJ-B-1.19/0.59 by 22%. At catenary action stage, the peak tension forces in CMJ-B-1.19/0.59 and EMJ-B-1.19/0.59 were 199.0 kN and 200.4 kN, respectively. Even though moment resistance of the beam was significantly reduced by severe crushing of concrete in the compression zone of the beam, the beam could transfer vertical load to the support through its tension resistance prior to fracture of top reinforcement near the end column stub.

5. Pseudo-Static Resistance of Sub-Assemblages

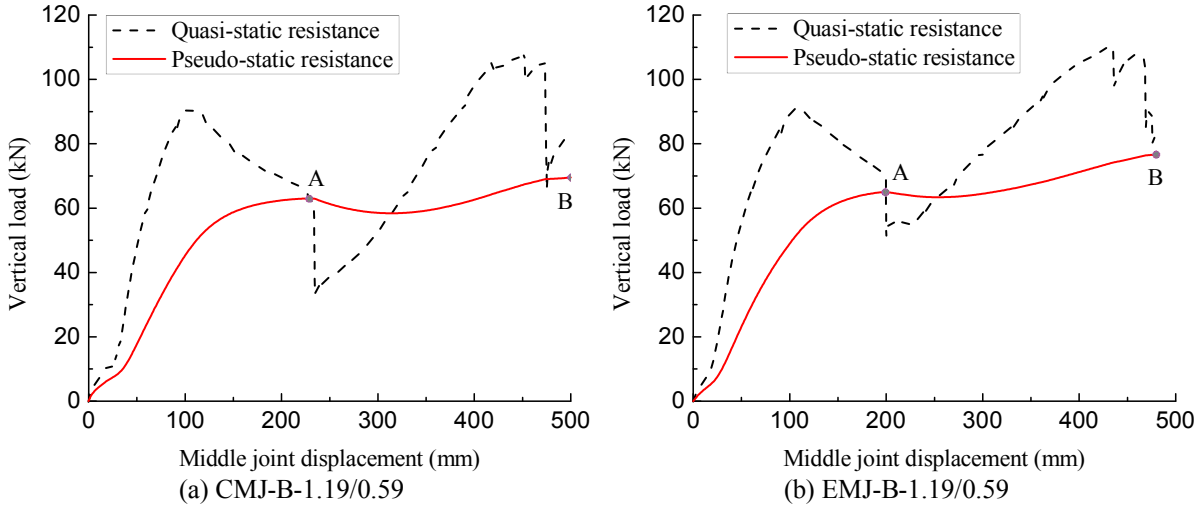

Fig. 6: Pseudo-static resistance of beam-column sub-assemblages

In addition to quasi-static resistance of sub-assemblages under column removal scenarios, pseudo-static resistance can also be calculated based on the energy balance method [12]. It is assumed that the work done by external loads is equal to the strain energy stored in the sub-assemblage. At a given vertical displacement, total work done by external load can be determined as the area under the load-displacement curve. When the same vertical displacement is attained under pseudo-static loading condition, the associated pseudo-static load can be calculated as the total work done by external load

divided by the vertical displacement. Thus, at each vertical displacement, pseudo-static resistance of sub-assemblages can be quantified through the quasi-static load-displacement curve. Fig. 6 shows the pseudo-static resistances of sub-assemblages CMJ-B-1.19/0.59 and EMJ-B-1.19/0.59. The maximum pseudo-static loads at compressive arch action and catenary action stages are 63.0 kN and 69.5 kN, respectively, for concrete sub-assemblage CMJ-B-1.19/0.59. EMJ-B-1.19/0.59 is able to sustain slightly greater pseudo-static load at compressive arch action stage. However, at catenary action stage, the maximum pseudo-static load is 76.6 kN, about 10% greater than that of CMJ-B-1.19/0.59. It is due to a less reduction in quasi-static load caused following fracture of bottom reinforcement at the middle joint, as shown in Fig. 5(a). Besides pseudo-static resistances, the ratio of the quasi-static resistance to the pseudo-static resistance of sub-assemblages is calculated, as listed in Table 3. The greater the ratio, the poorer the energy-absorption capacity of the sub-assemblage would be. As for sub-assemblages CMJ-B-1.19/0.59 and EMJ-B-1.19/0.59, the ratios at compressive arch action stage are close to one another. However, when the catenary action capacity was attained, the ratio for EMJ-B-1.19/0.59 is 1.56, significantly greater than that for CMJ-B-1.19/0.59. Thus, sub-assemblage EMJ-B-1.19/0.59 exhibits a better energy-absorption capacity compared to CMJ-B-1.19/0.59.

Table 3: Resistance of beam-column sub-assemblages

Sub-assemblages	CAA capacity (kN)			Catenary action capacity (kN)		
	Quasi-static P_c	Pseudo-static Q_c	P_c/Q_c	Quasi-static P_t	Pseudo-static Q_t	P_t/Q_t
CMJ-B-1.19/0.59	90.4	63.0	1.43	108.2	69.5	1.56
EMJ-B-1.19/0.59	91.1	65.1	1.40	110.3	76.6	1.44

6. Crack patterns and failure modes of bridging beam

Under column removal scenarios, conventional concrete and ECC sub-assemblages developed different crack patterns at the end column stub and the curtailment point of top reinforcement. In CMJ-B-1.19/0.59, fan-shaped cracks were observed at the beam end, and crushing and spalling of concrete occurred in the compression zone of the beam, as shown in Fig. 7(a). Besides, a partial hinge was formed at the curtailment point of beam top reinforcement (see Fig. 7(b)), which contributed a considerable portion to total deformation of the beam. Bottom reinforcement fractured at the face of the middle joint, as shown in Fig. 7(c). When concrete in structural topping and beam-column joints was replaced by ductile ECC, multiple cracking developed in the structural topping at the initial stage, as shown in Fig. 8(a). However, crack width remained at around 0.1 mm, indicating that ECC was effective in transferring tensile stresses through the bridging strength of fibres. With increasing middle joint displacement, major cracks were formed near the end column stub, and the strain capacity of ECC topping was exhausted at the crack plane. Away from the major cracks, ECC was still able to sustain tensile stresses. Special attention was given to the crack pattern at the curtailment point of beam top reinforcement. Due to strain-hardening behaviour of ECC in tension, limited cracks were observed at the curtailment point (see Fig. 8(b)). Similar failure mode to CMJ-B-1.19/0.59 was observed in the middle joint of EMJ-B-1.19/0.59, as shown in Fig. 8(c).

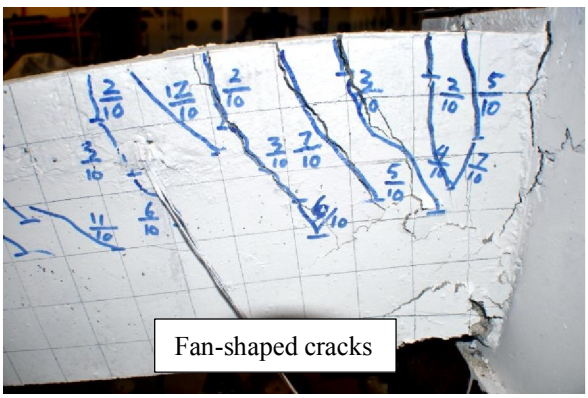

(a) In plastic hinge region

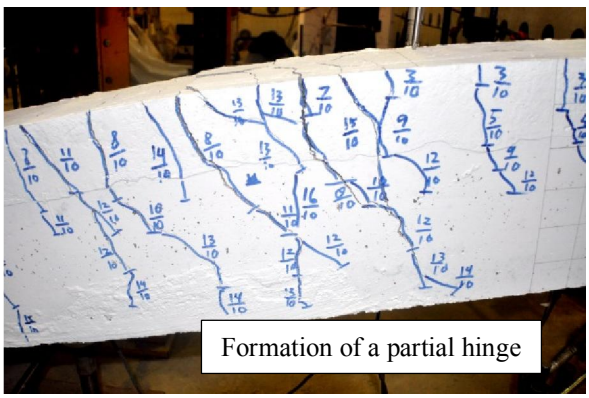

(b) At curtailment point of top reinforcement

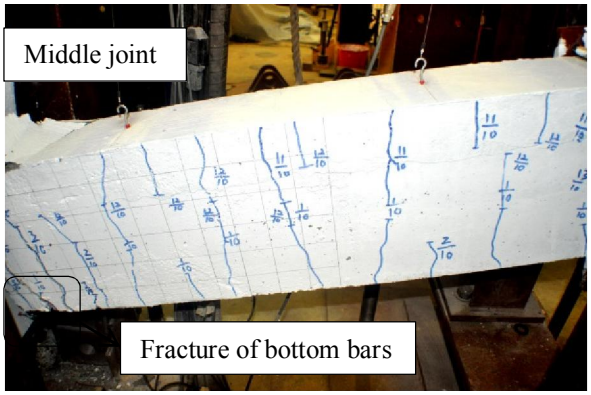

(c) At middle joint

Fig. 7: Crack pattern and failure mode of CMJ-B-1.19/0.59

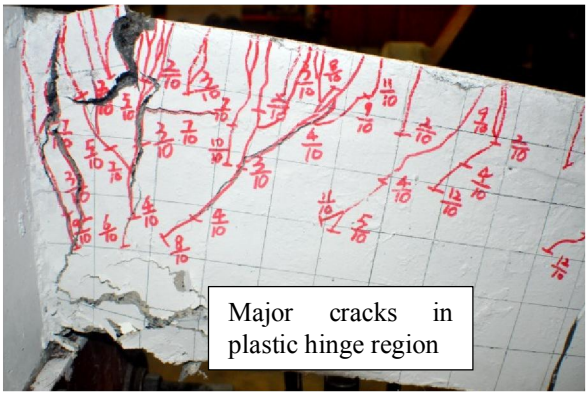

(a) In plastic hinge region

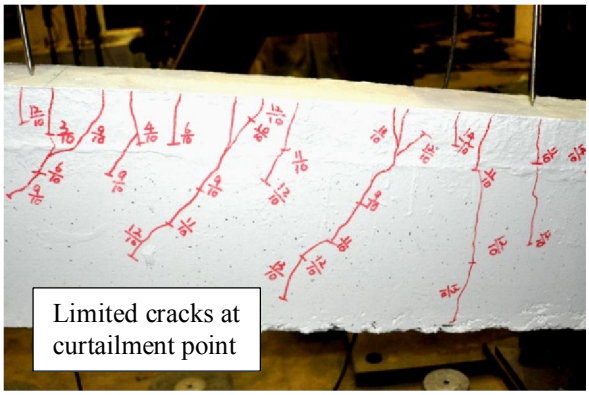

(b) At curtailment point of top reinforcement

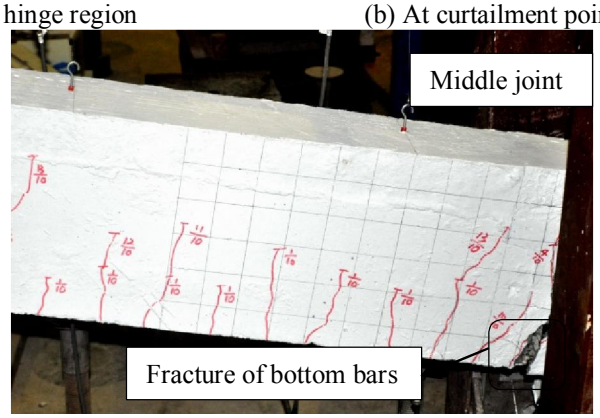

(c) At middle joint

Fig. 8: Crack pattern and failure mode of EMJ-B-1.19/0.59

The different crack patterns between concrete and ECC sub-assemblages resulted from the tension-stiffening behaviour of reinforced ECC members subjected to tension, as reported by Moreno [6]. After the formation of major cracks near the end column stub, ECC in structural topping tended to localise deformations of the beam in a limited region, as shown in Fig. 8(a). In addition to the crack pattern at the beam end, the effect of ECC on the deformation of sub-assemblage can also be demonstrated by the measured plastic hinge rotations, as discussed in the following section.

7. Rotations of plastic hinges

In the experimental test, plastic hinge rotations at the end column stub were measured through LVDTs, as shown in Fig. 3. Two rows of LVDTs were installed in the plastic hinge region. LE-1 and LE-2 measured rotation θ_1 of beam segment between the face of the end column and section S1, and LE-3 and LE-4 measured rotation θ_1 between sections S1 and S2. When the catenary action capacity

was attained, total rotations measured in a length of 270 mm were 6.5° and 6.9° for sub-assemblages CMJ-B-1.19/0.59 and EMJ-B-1.19/0.59, respectively. Besides the total rotations in the plastic hinge region, ratio γ_θ of θ_1 to $\theta_1+\theta_2$ is calculated, as shown in Fig. 9. The ratio can be interpreted as the degree of rotation localisation at the beam end. The greater the ratio, the more localised the rotations would be at the face of the end column stub. As for concrete sub-assemblage CMJ-B-1.19/0.59, the maximum ratio was obtained at compressive arch action stage, as shown in Fig. 9(a). Thereafter, the ratio was kept decreasing until catenary action commenced in the bridging beam. At catenary action stage, the ratio was nearly constant at 0.74. However, in sub-assemblage EMJ-B-1.19/0.59, the ratio increased with middle joint displacement at catenary action stage, as shown in Fig. 9(b). The maximum value was around 0.90, indicating that more severe localisation of rotations was obtained in EMJ-B-1.19/0.59 compared to CMJ-B-1.19/0.59. The localisation of rotations could be worse when the top reinforcement ratio in the beam is lower than 1.19%.

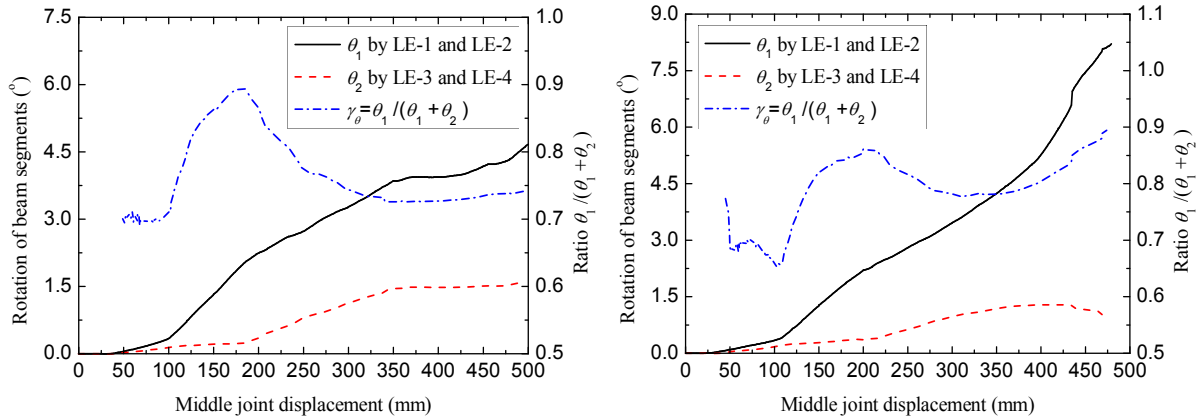

(a) CMJ-B-1.19/0.59 (b) EMJ-B-1.19/0.59

Fig. 9: Variations of plastic hinge rotations at beam end

8. Conclusions

In the experimental programme, two precast beam-column sub-assemblages were tested under quasi-static loading condition to study the behaviour under column removal scenarios. 90° bend of bottom reinforcement was employed in the middle joint. Conventional concrete and ECC were used in structural topping and beam-column joints of the sub-assemblages. Conclusions are obtained through comparisons between concrete and ECC sub-assemblages.

(1) Beam-column sub-assemblages CMJ-B-1.19/0.59 and EMJ-B-1.19/0.59 were able to develop significant compressive arch action and subsequent catenary action under column removal scenarios. However, the enhancement of ECC to structural resistance was insignificant under quasi-static loading condition.

(2) Compared to concrete specimen CMJ-B-1.19/0.59, around 10% greater pseudo-static resistance of ECC sub-assemblage EMJ-B-1.19/0.59 is obtained at catenary action stage. It is due to a better energy-absorption capacity of ECC sub-assemblage EMJ-B-1.19/0.59 in comparison with CMJ-B-1.19/0.59.

(3) Different crack patterns were observed in CMJ-B-1.19/0.59 and EMJ-B-1.19/0.59. Fan-shaped cracks developed in the plastic hinge region of CMJ-B-1.19/0.59, whereas ECC topping in EMJ-B-1.19/0.59 led to localisation of major cracks near the end column stub. It resulted from the tension-stiffening behaviour of ECC after the formation of major cracks in the plastic hinge region.

Acknowledgements

The authors acknowledge the support for the research project “Integrated Structures and Materials Design for Precast Concrete 66 kV Substation against Progressive Collapse” provided by JTC Corporation, Singapore.

References

[1] Yu J, Tan KH. Experimental and Numerical Investigation on Progressive Collapse Resistance of Reinforced Concrete Beam Column Sub-assemblages. Engineering Structures. 2013;55:90-106.
[2] Main JA, Bao Y, Lew HS, Sadek F. Robustness of Precast Concrete Frames: Experimental and Computational Studies. Structures Congress 20142014. p. 2210-20.
[3] FIB. Seismic design of precast concrete building structures. Bulletin 27: Fédération internationale du béton, Laussane, Switzerland; 2003.
[4] Li VC. On Engineered Cementitous Composites (ECC)-A Review of the Material and Its Applications Journal of Advanced Concrete Technology. 2003;1:215-30.
[5] Fischer G, Li VC. Influence of Matrix Ductility on Tension-Stiffening Behavior of Steel Reinforced Engineered Cementitious Composites (ECC). ACI Structural Journal. 2002;99:104-11.
[6] Moreno DM, Trono W, Jen G, Ostertag C, Billington S. Tension Stiffening in Reinforced High Performance Fiber Reinforced Cement-Based Composites. Cement & Concrete Composites. 2014;50:36-46.
[7] BSI. Eurocode 2: Design of concrete structures—Part 1-1: General rules and rules for buildings. BS EN 1992-1-1:2004: British Standards Institution, London; 2004. p. 225.
[8] DOD. Design of Buildings to Resist Progressive Collapse. Unified Facilities Criteria(UFC) 4-023-03: Department of Defence, Washington, DC; 2013.
[9] Van Acker A. Accidental Actions and Progressive Collapse. International Seminar on Precast Concrete Structures: Department of Civil Engineering Universidade Nova de Lisboa; 2013.
[10] Qian S, Li VC. Simplified Inverse Method for Determining the Tensile Strain Capacity of Strain Hardening Cementitious Composites. Journal of Advanced Concrete Technology. 2007;5:235-46.
[11] Qian S, Li VC. Simplified Inverse Method for Determining the Tensile Properties of Strain Hardening Cementitious Composites (SHCC). Journal of Advanced Concrete Technology. 2008;6:353-63.
[12] Izzudin BA, Vlassis AG, Elghazouli AY, Nethercot DA. Progressive collapse of multi-storey buildings due to sudden column loss - Part I: Simplified assessment framework. Engineering Structures. 2008;30:1308-18.